Anomalous phonon properties in the silicide superconductors CaAlSi and SrAlSi

S. Kuroiwa,[1] T. Hasegawa,[2] T. Kondo,[3] N. Ogita,[2] M. Udagawa,[2] and J. Akimitsu[1]
[1]*Department of Physics and Mathematics, Aoyama Gakuin University, Fuchinobe 5-10-1, Sagamihara, Kanagawa 229-8558, Japan*
[2]*Graduate School of Integrated Arts and Sciences, Hiroshima University, Kagamiyama 1-7-1, Higashi-Hiroshima, Hiroshima 739-8521, Japan*
[3]*Venture Business Laboratory of Hiroshima University, Kagamiyama 2-313, Higashi-Hiroshima, Hiroshima 739-8527, Japan*
(Received 3 April 2008; revised manuscript received 29 July 2008; published 10 November 2008)

Lattice-dynamical properties of CaAlSi and SrAlSi with a similar layer structure to MgB_2 have been first investigated by both Raman-scattering and *ab initio* calculations. All Raman-active phonons with E' symmetry have been clearly observed for both compounds. Their line shapes are asymmetric but their linewidths are $\sim 10\ cm^{-1}$, which is very narrower than that of MgB_2. In addition to the Raman-active modes, several extra peaks have been observed below $160\ cm^{-1}$. These low-energy extra modes can be assigned to the out-of-plane vibrations of Al perpendicular to Al-Si basal plane. Since these peak intensities are strongly affected by the incident energy (resonance Raman process), the electronic state is important for them. Moreover, in both crystals of CaAlSi and SrAlSi, we point out the energy difference for the different propagation directions along the c axis and the c plane, in spite of the very close wave vector to the Brillouin-zone center. This energy difference cannot be explained by a usual Raman-scattering scenario at this stage.

DOI: 10.1103/PhysRevB.78.184303 PACS number(s): 78.30.−j, 74.25.Kc, 74.70.Dd

I. INTRODUCTION

The discovery of superconductivity in MgB_2 (Ref. 1) has refocused attention on phonon-mediated superconductor for the development of new materials with higher superconducting transition temperature (T_c). For MgB_2, the high-frequency optical E_{2g} mode (B-B bond-stretching vibration) is selectively and strongly coupled with electrons on σ-band Fermi surface,[2,3] although the average electron-phonon coupling (EPC) for full Fermi surface is rather moderate.[4,5] This peculiar feature of electron-phonon interaction is considered as an important nature for the high T_c of MgB_2.

In MgB_2, the E_{2g} phonon measured by Raman scattering appears around $600\ cm^{-1}$ with very broad linewidth of $250-300\ cm^{-1}$ at room temperature. At low temperatures, the linewidth clearly narrows to $170\ cm^{-1}$ and the frequency shows a slight hardening of about $10\ cm^{-1}$.[6–8] Among these anomalous behaviors, line broadening with increasing temperature might be ascribed by a large anharmonic contribution, while the broad linewidth at low temperatures is not due to anharmonicity but to the strong electron-phonon interaction.[9,10]

Important EPC knowledge in MgB_2 obtained by Raman scattering suggests that the similar studies for the analogous intermetallic compounds such as alkaline-earth-intercalated graphite[11] and ternary silicide MAlSi (M: alkaline-earth atoms)[12,13] are necessary in order to gain an insight into the electron-phonon pairing mechanism of superconductivity as a reference material for MgB_2.

Recently Sagayama *et al.*[14] have reported two types of CaAlSi: fivefold (5H-CaAlSi) and sixfold (6H-CaAlSi) superstructure along the c axis. Very recently, a simpler structure without any c-axis superstructure has been found for CaAlSi (1H-CaAlSi) (Ref. 15) and SrAlSi (Ref. 16) in addition to the multistacked structures of CaAlSi. The structure of 1H-CaAlSi and SrAlSi is similar to that of MgB_2, but the B_2 layer of MgB_2 is replaced by that constructed by Al and Si. As a result, its space group becomes $P\bar{6}m2$, which is different from $P6/mmm$ of MgB_2. In 1H-CaAlSi, Ca and AlSi planes are alternately stacked along the c axis, but the AlSi plane is distorted for 5H-CaAlSi and 6H-CaAlSi. It is notable that T_c and other transport properties depend on the distorted sequence of AlSi planes among the three structures of CaAlSi.[15] 1H-CaAlSi and SrAlSi with the similar structure to MgB_2 are investigated in this paper.

Theoretical calculations on the phonon dynamics of 1H-CaAlSi have suggested that superconductivity is dominated by EPC with a low-energy phonon mode, which is the out-of-plane displacement of Al at Brillouin-zone boundary including A-L-H-A path.[17–19] In fact, the recent generalized phonon density of states (GDOS) measured by inelastic neutron scattering gives us the evidence of soft-mode behavior in polycrystalline CaAlSi.[20] Therefore, this silicide system is very interesting not only for the comparison with superconducting properties of MgB_2 but also for the investigation of its own lattice-dynamical properties. However, in spite of various investigations so far,[20–25] there is very little experimental knowledge on the lattice-dynamical properties and EPC mechanism in 1H-CaAlSi and SrAlSi.

In this paper, we present systematic results of Raman-scattering and of *ab initio* calculations for the lattice dynamics for 1H-CaAlSi and SrAlSi. Two modes with the E' symmetry are Raman active according to the group theoretical analysis for $P\bar{6}m2$. This lowered symmetry than that of MgB_2 activates the low-energy E' (E'_{low}: in-plane displacement between the Ca/Sr plane and the AlSi plane) mode in addition to the high-energy E' (E'_{high}: in-plane Al-Si bonding motion) mode. The latter mode corresponds to the E_{2g} mode in MgB_2. Our present results indicate that the two Raman-active phonons of 1H-CaAlSi and SrAlSi have been observed and assigned to the E' representation by their polarization dependences. Their spectra exhibit asymmetric line

shapes with linewidth of 10–20 cm^{-1}. This spectral feature is markedly different from that of MgB_2. Thus, EPC for E'_{high} mode in these silicides seems to be smaller than that in MgB_2 as expected from the theoretical calculations.[20] Interestingly, we have clearly observed the various anomalous spectra such as low-energy extra modes (LEMs) in addition to the Raman-active phonons and have found an anomalous energy difference near the zone center for the different propagation direction.

The present paper focuses on the anomalous phonon properties observed in this investigation and this paper is organized as follows. We first describe detailed experimental conditions and *ab initio* calculation procedures in Sec. II. Section III shows experimental results obtained from polarization, excitation energy, and temperature dependences of Raman-scattering measurements. Finally, we discuss the origin of the observed phonon modes by the comparison between the experimental and *ab initio* calculation results in Sec. IV.

II. EXPERIMENTS AND CALCULATIONS

Single crystals of 1*H*-CaAlSi and SrAlSi were synthesized by a floating zone method. Detailed growth conditions and superconducting properties were described in Refs. 15 and 16. The obtained ingots were confirmed to be single-crystal form and had no superlattice reflections from synchrotron x-ray Laue patterns and neutron-diffraction patterns on the (00*l*) lines in the reciprocal lattice. They turned out to have a hexagonal unit cell with $P\bar{6}m2$ symmetry and they did not include superlattice structure.

Raman-scattering experiments under backscattering geometry were performed using a triple monochromator (JASCO model NR-1800), and analyzed light was detected by a liquid N_2 cooled charge-coupled device (CCD) detector (Princeton Instruments Inc. model LN/CCD-1100-PB). Wavelengths of incident beam were 457.9–514.5 nm and 568.2–647.0 nm of Ar and Kr laser, respectively, and the output power was 10 mW. Raman-scattering geometry is defined by a symbol $k_i(p_i,p_s)k_s$, where k and p are directions of propagation and polarization of laser or scattered light, respectively. The subscripts i and s represent incident and scattered lights, respectively. In this work, a and c correspond to the crystallographic axes of [100] and [001], respectively, and b^* is in a direction perpendicular to [100] and [001] in the hexagonal symmetry.

Number of phonons at Brillouin-zone center has been determined by a factor group analysis in $P\bar{6}m2$ space group as $2A''_2+2E'$. Two nondegenerate A''_2 phonon modes are infrared-active modes with the displacements of all atoms along the c axis. Two doubly degenerate E' modes are infrared and Raman actives. The Raman-active E' modes appear in the polarization geometries of (a,a), (a,b^*), (b^*,a), and (b^*,b^*).

Ab initio calculations have been performed on 1*H*-CaAlSi and SrAlSi using ABINIT code,[26,27] which is based on *ab initio* pseudopotentials and a plane-wave basis set in the framework of the density-functional theory. The local-density approximation was adopted for exchange-correlation energy and the exchange-correlation energy presented by Perdew and Wang[28] was used. The Troullier-Martins-type[29] pseudopotentials are generated using the FHI98PP code.[30] Ca and Sr pseudopotentials include ten electrons for valence states, i.e., they include inner s and p states in addition to outer s states. A cutoff energy of plane-wave basis set is 42 Ry, where 1 Ry=13.606 eV. For an integration of the Brillouin zone, special points[31,32] on $12\times12\times8$ **k**-point grids with a smearing width of 0.02 Ry were used. Calculations of lattice dynamics were performed within the density-functional perturbation theory.[33,34] To obtain interatomic force constants and phonon-dispersion curves, the Fourier interpolation method was used on $6\times6\times4$ grids. Density of states was calculated by tetrahedron method[35,36] using $24\times24\times24$ grids. Structures were optimized from the reported structure data[15] and lattice-dynamical calculation has been performed for the optimized structures. The obtained lattice parameters are a=4.141 Å and c=4.274 Å for 1*H*-CaAlSi and a=4.188 Å and c=4.582 Å for SrAlSi.

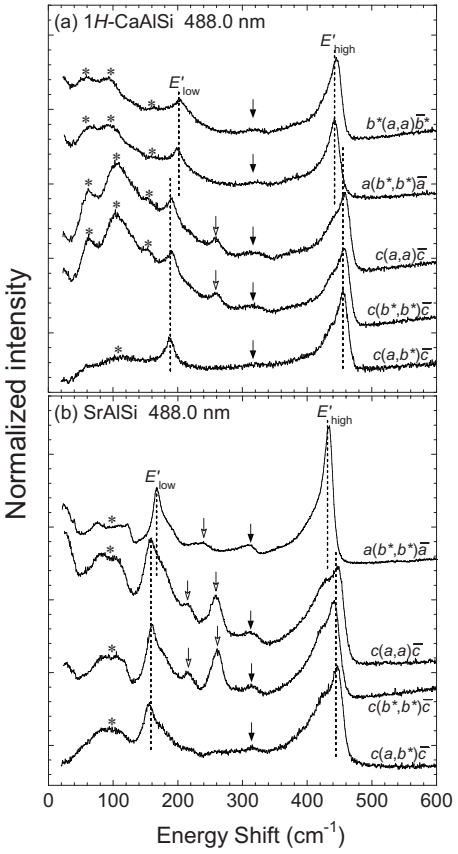

FIG. 1. Polarization dependence of Raman spectra of 1*H*-CaAlSi and SrAlSi at room temperature with the incident wavelength of 488.0 nm. The arrows and asterisks denote the two-phonon excitation and LEM, respectively.

III. EXPERIMENTAL RESULTS

A. Overview of 1*H*-CaAlSi and SrAlSi

Figure 1 shows the polarization dependence of Raman spectra for (a) 1*H*-CaAlSi and (b) SrAlSi measured with the

incident wavelength of 488.0 nm at room temperature. In the figure, the energy region between 20 and 600 cm^{-1} is shown, since no sign of any excitation peak has been observed from 600 to 1200 cm^{-1}. For both compounds, the number of the observed peaks is larger than two, which is the number of the Raman-active phonons for one-phonon scattering process.

We point out here two peaks at around 200 and 450 cm^{-1} for 1*H*-CaAlSi and 160 and 440 cm^{-1} for SrAlSi. They are clearly observed in the polarization geometry of (a,a), (a,b^*), and (b^*,b^*) as shown in Fig. 1, while there is no E' phonon modes for the (c,a) and (c,c) spectra (not shown in this paper). Therefore, we conclude that these two peaks are the phonons with the E' symmetry from the polarization selection rule in the $P\bar{6}m2$ symmetry. These assigned peaks are depicted by E'_{low} and E'_{high} in Fig. 1.

We now focus on the E'_{high} phonon spectra corresponding to the E_{2g} modes in MgB_2. Comparison of the present data with the Raman spectra of MgB_2 shows that the line shapes of E'_{high} modes are clearly asymmetric and their linewidths are much smaller than that of MgB_2.[7] Such a small linewidth in 1*H*-CaAlSi and SrAlSi implies that the EPC for E'_{high} mode in these silicides is significantly suppressed in comparison with that for the E_{2g} modes in MgB_2.[7] Meanwhile, asymmetric line shapes with the linewidth of ~ 10 cm^{-1} observed in 1*H*-CaAlSi and SrAlSi are attributed to the Fano effect,[37,38] which is the interference effect between a discrete phonon excitation and a continuum electronic excitation. In the Fano model, an asymmetric spectrum is written as

$$I_F \frac{(q+\varepsilon)^2}{1+\varepsilon^2}, \tag{1}$$

where $\varepsilon=(\omega-\omega_p)/\Gamma$. ω, ω_p, Γ, I_F, and q are Raman frequency shift, phonon frequency, linewidth of the phonon excitation, scattering intensity, and asymmetric parameter, which is proportional to inverse of electron-phonon interaction. By fitting this function to two E' modes with a linear background, we find that the Fano model can reproduce the experimental spectra for all E' mode but that the parameter q strongly depends on background shapes. As discussed later, the overall spectra and line shapes vary with wavelength and scattering geometries. Therefore, we cannot obtain reliable parameter q for each peak and we do not discuss the parameter q in this paper. Here, we show typical parameter q, which is obtained from $a(b^*,b^*)\bar{a}$ spectra. The obtained parameter q is -3.0, -3.5, and 11 for E'_{high} of 1*H*-CaAlSi, E'_{high} of SrAlSi, and E'_{low} of SrAlSi, respectively. The q for E'_{low} of 1*H*-SrCaAlSi is too large to determine accurately. In fact, this peak is almost symmetric and close to Lorenzian line shape. As seen from line shape and these parameters, EPC of E'_{high} mode is larger than those of E'_{low}, and the sign of q, i.e., electron-phonon interaction, is opposite for both modes.

The most peculiar observation in Fig. 1 is the different energies of E'_{high} and E'_{low} between $c(*,*)\bar{c}$ and $a(*,*)\bar{a}/b^*(*,*)\bar{b}^*$ for both compounds (here $*=a$ or b^*). As seen in Fig. 1, we observe the same E' symmetry phonons with slightly different wave vector. In the ordinary case, these phonons should have the same energy since scattering vectors are very small with respect to the reciprocal-lattice vectors in Raman-scattering measurements. However, the present result is not the ordinary case.

We can think two origins for this anomalous result. One is that very small difference in wave vector causes quite large energy difference in the E' modes in these compounds. The other one is originated from different structures on different surfaces. Since light can penetrate a metal by a small distance, if the deformation of surface structure is diffused to this distance, Raman-scattering spectra from such distorted surfaces become different.

In addition to above two origins, we may imagine a difference between longitudinal optical (LO) and transverse optical (TO) modes as seen in a piezoelectric compound. However, the LO-TO scenario is not applicable to the present case because the compounds are conducting. Since conduction electrons can screen macroscopic electric field, which is necessary to produce splitting between degenerated LO and TO modes, there is no energy difference between these modes in conducting compounds. Notwithstanding, it is worth to check the LO and TO modes for the E' phonons. In these compounds, we can observe the LO modes of the E' modes only in $b^*(a,a)b^*$ spectra, while the TO modes can be found in $c(a,a)\bar{c}$, $c(b^*,b^*)\bar{c}$, $c(a,b^*)\bar{c}$, and $a(b^*,b^*)\bar{a}$ spectra. Since $b^*(a,a)b^*$ and $a(b^*,b^*)\bar{a}$ geometries show the same energy for 1*H*-CaAlSi, we conclude that the different energy is not invoked by macroscopic electric-field. Thus, we have two interpretations of the different spectra for $c(*,*)\bar{c}$ and $a(*,*)\bar{a}/b^*(*,*)b^*$, i.e., deformation of surface structure and different scattering vectors. Here, we note some characteristics of the difference and the discussion of two possibilities will be described in Sec. IV.

Although the energy differences have been found between $c(b^*,b^*)\bar{c}$ and $a(b^*,b^*)\bar{a}$, a striking difference is the line shapes of E'_{low} and E'_{high}. For 1*H*-CaAlSi, the line shapes of the E'_{high} phonon mode is doublet for $c(b^*,b^*)\bar{c}$, while those of E'_{low} for both spectra and those of E'_{high} in $a(b^*,b^*)\bar{a}$ can be reproduced by single component. Meanwhile, the spectral shapes in SrAlSi are slightly different from those of 1*H*-CaAlSi, i.e., E'_{low} show doublet shape. As seen here for E' modes, many observed peaks exhibit quite complicated and different shapes for $c(b^*,b^*)\bar{c}$ and $a(b^*,b^*)\bar{a}$. Therefore, we determined the phonon energy by the energy at the top of the peak.

Several extra peaks marked by asterisks and open and closed arrows appear in both compounds, in addition to the Raman-active E' phonons, and strongly appear in (a,a), (b^*,b^*), and (c,c). These extra peaks depicted by arrows can be originated from a two-phonon scattering and assigned as the A_1 symmetry. Two-phonon scattering will be found around twice of the energy of large phonon DOS. As seen later (Fig. 6), calculated DOS shows large peaks around 120, 170, and 440 cm^{-1} for 1*H*-CaAlSi and around 65, 110, 160, and 415 cm^{-1} for SrAlSi. Therefore, the extra peaks around 320 cm^{-1} for 1*H*-CaAlSi and SrAlSi, denoted by closed arrows in Fig. 1, are assigned to the excitations of two phonons around 170 cm^{-1} (1*H*-CaAlSi) or 160 cm^{-1} (SrAlSi). The peaks around 260 cm^{-1} for both compounds (open arrows) may be considered as two-phonon scattering. However, the peaks exhibit clear difference between $c(*,*)\bar{c}$ and

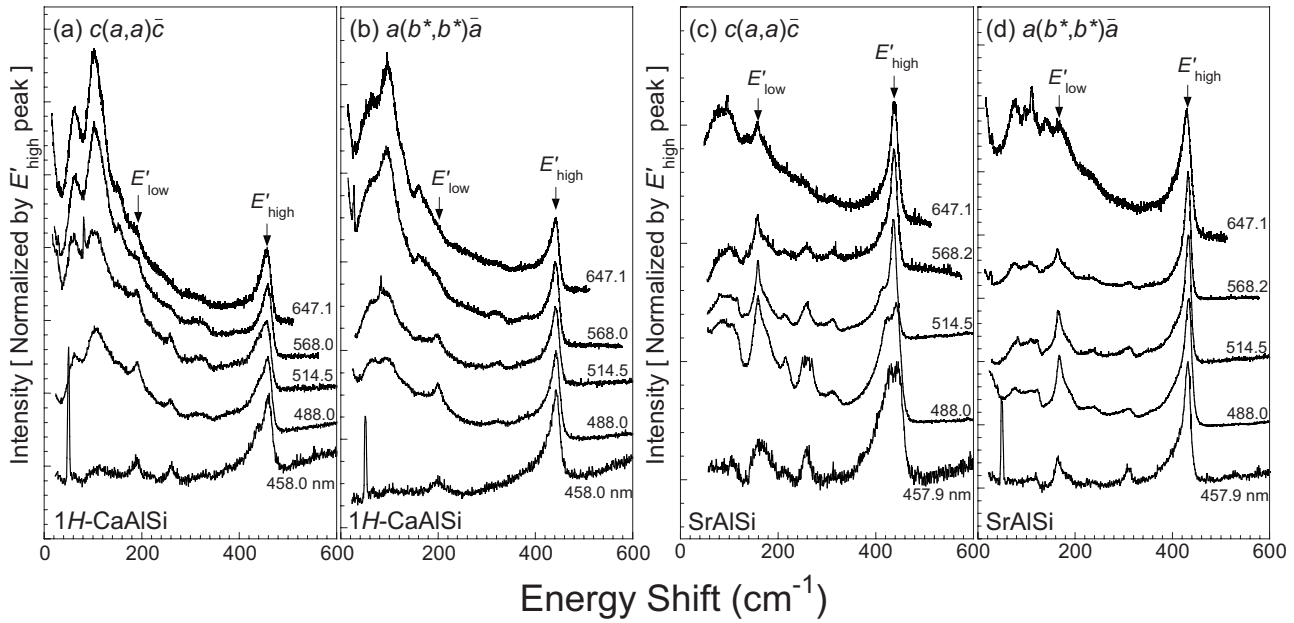

FIG. 2. Excitation energy dependence of typical Raman spectra at room temperature for the polarization geometry of (a) $c(a,a)\bar{c}$ and (b) $a(b^*,b^*)\bar{a}$ of 1*H*-CaAlSi and (c) $c(a,a)\bar{c}$ and (d) $a(b^*,b^*)\bar{a}$ of SrAlSi. The intensity of all spectra is normalized by that of each E'_{high} mode and the sharp peaks at low energy are due to the natural emission.

$a(*,*)\bar{a}/b^*(*,*)b^*$ geometries. We do not deal with these peaks in this paper since this anomalous feature makes the origin of these peaks very difficult to discuss.

The low-energy extra excitations below 160 cm^{-1} depicted by asterisks also show some differences between the $c(b^*,b^*)\bar{c}$ and $a(b^*,b^*)\bar{a}$ geometries. At this stage, the determination of their origins is difficult within few experimental results. However, there are some hints to clarify their origins. One is that their too low energies and profiles of peaks can discard two-phonon scattering. Another one is, as seen in Sec. IV, that their peaks exhibit characteristic resonance effect in intensity. We will discuss an origin of the low-energy modes (LEMs) using these evidences in Sec. IV.

We stress here that the displayed Raman spectra in this paper are well reproducible and were obtained from several other single-crystalline specimens. Moreover, we can determine the absolute value of the energy shift with an accuracy of 1.4 cm^{-1} in the present experimental setup. In particular, we calibrated the accuracy of experimental energy shift for all spectra by using natural emission of He-Ne laser. Therefore, the anomalous differences of spectra are not due to experimental error but due to intrinsic properties in this system.

B. Excitation energy dependence

Purposes of the excitation energy dependence are: (i) to obtain a phonon dispersion in a narrow range near the Brillouin-zone center, (ii) to see an effect of resonance scattering, and (iii) to check a surface influence using various penetration depths of incident laser. The results of the excitation energy dependence at room temperature are shown in Fig. 2, where the representative polarization geometries of (a) $c(a,a)\bar{c}$ and (b) $a(b^*,b^*)\bar{a}$ of 1*H*-CaAlSi and (c) $c(a,a)\bar{c}$ and (d) $a(b^*,b^*)\bar{a}$ of SrAlSi are presented. The intensity of all spectra is normalized by that of each E'_{high} mode because we found that the intensity of E'_{high} mode is almost independent of excitation energy. As shown in panels (b) and (d), the line shape of E'_{high} phonon spectra for propagation direction to the in plane is almost independent of the excitation energy, while that for $c(a,a)\bar{c}$ is drastically changed from doublet to single component with increasing incident wavelength. In both compounds, the characteristics of E'_{low} spectra seem to be independent of the excitation energy. The intensity of LEMs extremely increases with increasing incident wavelength. Such a remarkable change in low-energy excitation is probably due to resonance effect with electronic excitation. Moreover, the extra peaks around 260 cm^{-1} and around 320 cm^{-1} also show the slight resonance effect.

Figure 3 shows the incident wavelength dependence of the peak energies of E'_{low}, E'_{high}, and LEMs at room temperature for 1*H*-CaAlSi and SrAlSi. Here, the energies of E' modes of both compounds are defined by that of spectral peak top. At the incident wavelengths of 568.2 and 647.1 nm, the energy of the E'_{low} mode for 1*H*-CaAlSi could not be deduced precisely because of strong intensity of the low-energy modes. The error bars of LEMs in 1*H*-CaAlSi correspond to the linewidth of broad peaks. For SrAlSi, the energy and error bars of LEMs are defined by the middle point and the width of trapezoidal-like spectra, respectively.

We note again that the peak energy of E'_{high} and E'_{low} depends on the propagation directions between the in-plane and the *c*-axis directions, but the direction of the energy shift is opposite between E'_{high} and E'_{low}. Furthermore, the extra peaks at 80–100 and 150–160 cm^{-1} in 1*H*-CaAlSi also show the propagation direction dependence as well as E', while those at 60 cm^{-1} do not show such dependence. As shown in Fig. 3, the energy of all peaks does not depend on

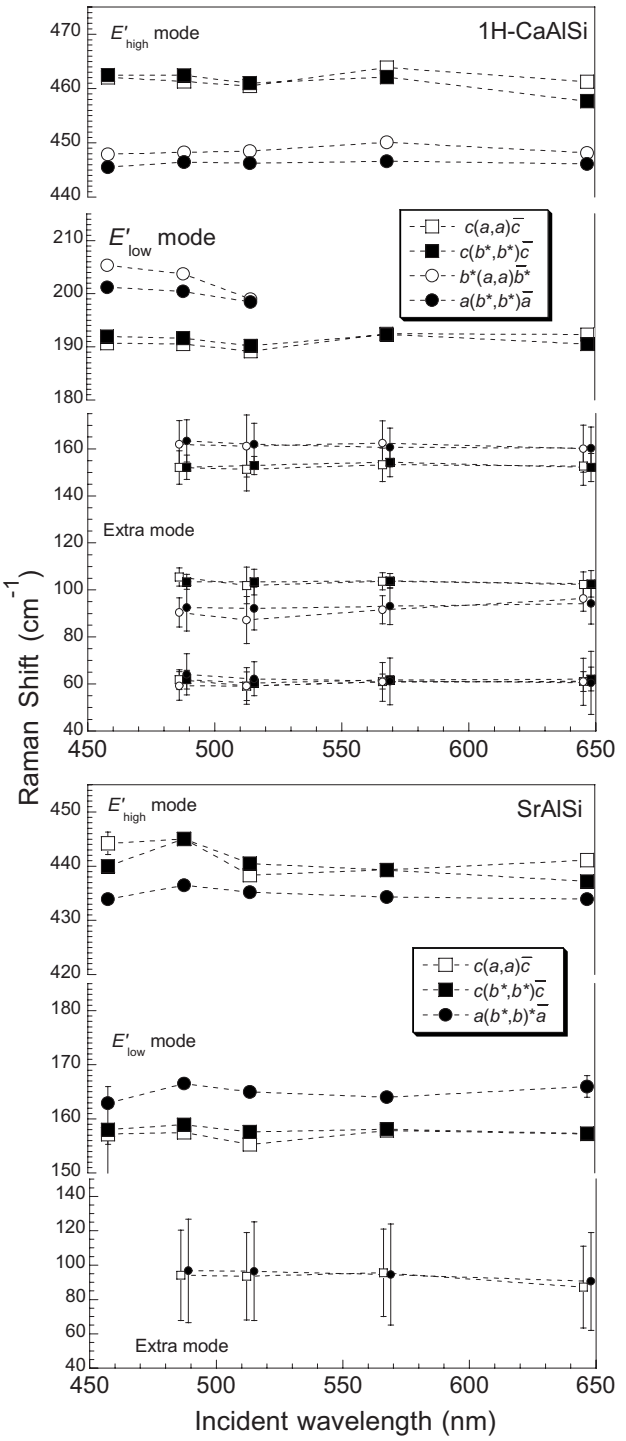

FIG. 3. The incident wavelength dependence of peak energy of E'_{low} and E'_{high} modes for 1H-CaAlSi and SrAlSi. The error bars of extra modes correspond to the linewidth of broad peak.

the incident-beam wavelength in the region of 458–647 nm. Therefore, at the level of the present data, there is no evidence for the presence of phonon energy dispersion in this wavelength region near the Brillouin-zone center.

C. Temperature dependence

The LEMs below 160 cm^{-1} exhibit a peculiar feature for the temperature variation while other phonon peaks show a

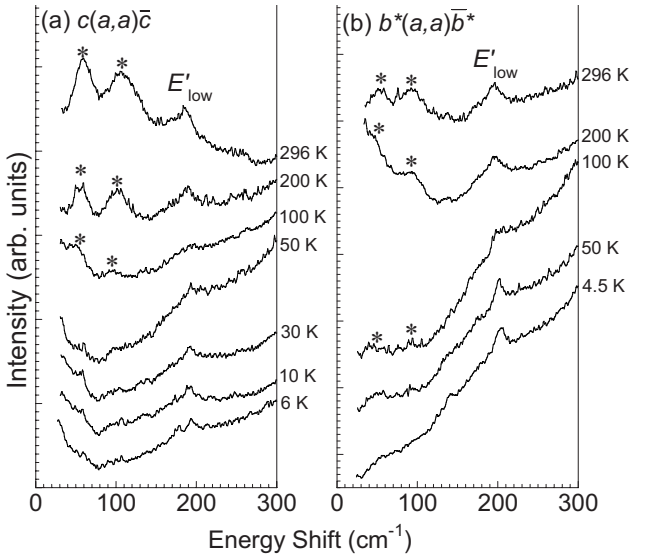

FIG. 4. Temperature dependence of Raman spectra below 300 cm^{-1} for 1H-CaAlSi with the incident wavelength of 514.5 nm. The panels (a) and (b) are the spectra for the polarization geometries of $c(a,a)\bar{c}$ and $b^*(a,a)\bar{b}^*$, respectively. The asterisk symbols denote the low-energy extra peaks.

usual temperature dependence. Figure 4 shows the temperature dependence of low-energy Raman spectra below 300 cm^{-1} for 1H-CaAlSi with the incident wavelength of 514.5 nm, where the panels (a) and (b) are the spectra for the polarization geometries of $c(a,a)\bar{c}$ and $b^*(a,a)\bar{b}^*$, respectively. As shown in Fig. 4, the intensity of LEMs denoted by asterisks decreases with the decrease in temperature and they are almost disappeared at the low temperature. On the contrary, the enhancements of gradient over the entire background with decreasing temperature were commonly observed in all propagation and polarization geometry. This behavior of the background is probably attributed to the impurity effect (e.g., fluorescence from surface-absorbed moisture), and thereby we think that they are not due to the intrinsic properties.

Figure 5 shows the temperature dependence of the peak energy for the E'_{low} and E'_{high} modes and LEMs in 1H-CaAlSi. Here, we could not extract the peak energy of LEMs with 150–160 cm^{-1} because of its weak intensity. The open square and circle indicate the data for the polarization geometries of $c(a,a)\bar{c}$ and $b^*(a,a)\bar{b}^*$, respectively. The respective E'_{low} and E'_{high} phonon energy increases with decreasing temperature due to the decrease in lattice constants, while their linewidth are constant on temperature (not displayed in this paper). The present results are remarkably different from the case of MgB_2, where the linewidth narrowing occurs from room temperature to low temperature and the resultant linewidth of 170 cm^{-1} at 5 K is caused by EPC.[7,8] For the present spectra, as mentioned above, the line shape can be explained by the interference effect with Fano type. Thus, a quite different EPC for the in-plane phonon modes near zone center are found between MgB_2 and CaAlSi/SrAlSi.

The energy difference between $c(a,a)\bar{c}$ and $b^*(a,a)\bar{b}^*$ is almost independent of temperature, and two E' phonon

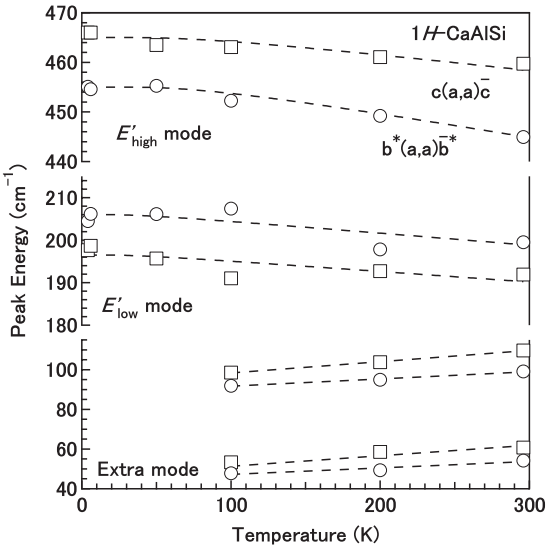

FIG. 5. Temperature dependence of the peak energy of E'_{low} and E'_{high} phonon modes and LEM for 1*H*-CaAlSi. The open circle and square symbols indicate data for the polarization geometries of $b^*(a,a)\bar{b}^*$ and $c(a,a)\bar{c}$. The dashed lines are guides for the eyes.

modes do not show the clear softening nor hardening around the superconducting transition temperature T_c. It is worthy to note that the peak energy of the extra modes anomalously decreases with decreasing temperature, which is markedly different from the usual temperature dependence. The details will be described in Sec. IV.

IV. DISCUSSION

A. LEMs

Here, we first discuss several possible origins of LEM in both compounds. We have clearly observed LEMs at around 50–60, 90–100, and 150–160 cm^{-1} in 1*H*-CaAlSi and 80–120 cm^{-1} in SrAlSi at the excitation wavelength from 488.0 to 647.1 nm. For both compounds, the relative intensity of LEMs decreases with decreasing incident wavelength and it completely vanishes at 457.9 nm. Therefore, LEMs are activated by a resonance effect not due to a locally lowered crystal symmetry such as translational symmetry breaking. When a resonant condition is satisfied, we can observe scattered light produced by higher-order process, which is very weak in an off-resonance condition. In the present case, the resonance is closely related to electronic excitations with energy below 2 eV because these intensities are clearly enhanced at 568.2–647.1 nm.

On the other hand, intensity of these low-energy extra peaks is significantly suppressed with decreasing temperature (as shown in Fig. 4). The variation in the intensity is much larger than that of the E'_{low} mode. Moreover, the linewidths of the LEMs do not vary largely and the spectral shapes seem to keep the line shapes of room temperature even at low temperatures. These features show that LEMs are not the direct electronic excitation since low-energy electronic excitations expected in metallic compounds with large bandwidths have no characteristic peak structure in Raman

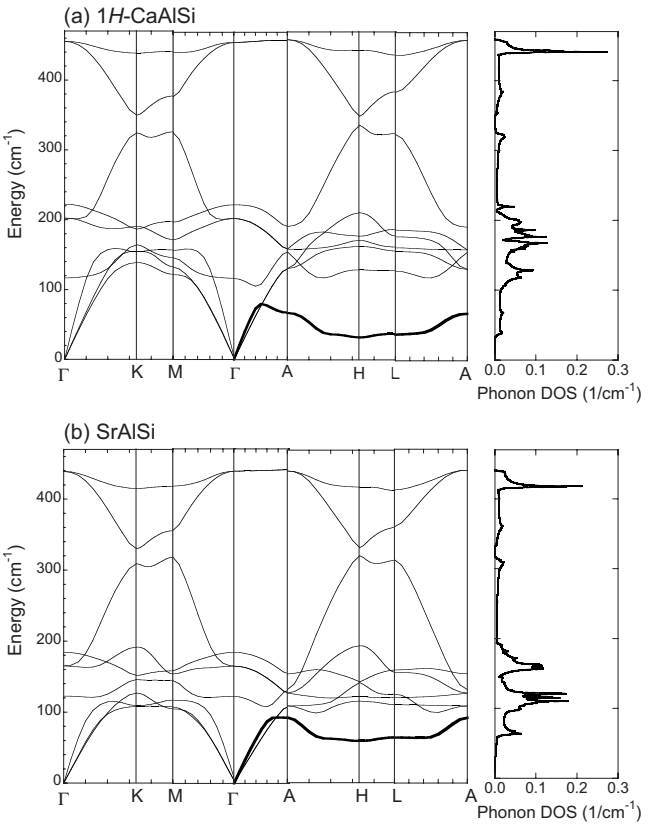

FIG. 6. Calculated phonon-dispersion curves and total phonon DOS (right panel) for (a) 1*H*-CaAlSi and (b) SrAlSi.

spectra. Therefore, we believe that the main part of the LEMs consists of phonon modes and that they can be activated by an assistance of other low-energy fluctuations through a resonant effect.

In order to clarify the origin of low-lying phonon modes, we have performed *ab initio* calculations for 1*H*-CaAlSi and SrAlSi. Figures 6 shows the overall phonon-dispersion curves and total phonon DOS of (a) 1*H*-CaAlSi and (b) SrAlSi and the partial phonon DOS (PDOS) for each atom and each direction is shown in Fig. 7. The phonon-dispersion curves and phonon DOS of 1*H*-CaAlSi and SrAlSi have been reported by other groups.[18–20] The present result for 1*H*-CaAlSi is similar to the reported ones[18,20] but different from the result reported by Huang *et al.*,[19] which has shown some unstable vibrations. Except for this small but important discrepancy these results agree with each other including DOS. DOS of each atom has been reported as GDOS by Heid *et al.*[20] Although GDOS cannot be directly compared with the present DOS, the peak energies of GDOS well agree with the present results in Fig. 7.

From the calculated DOS and PDOS, we can judge a possibility that an origin of the LEMs is a broken symmetry due to the structural distortion such as defects, dislocations, and stacking faults. Shapes of Raman spectra produced by structural distortions are in many cases similar to that of phonon DOS if the distortions affect all kinds of atoms or to that of PDOS if those affect one kind of atoms. Since the several peak structures below 160 cm^{-1} of the 1*H*-CaAlSi and SrAlSi spectra are inconsistent with any of calculated

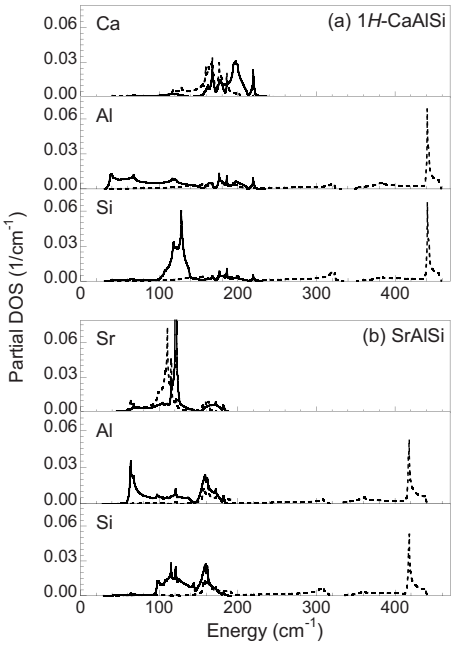

FIG. 7. Calculated partial phonon DOS of (a) 1*H*-CaAlSi and (b) SrAlSi. The dashed and solid lines correspond to each partial phonon DOS for in-plane and out-of-plane displacements, respectively.

DOS (see the right panel of Fig. 6) and PDOS (see also Fig. 7), it is unlikely that the presence of the LEMs is originated from structural distortions. Moreover, two-phonon scattering can be disallowed by the fact that the lowest energy of the LEMs is the same as the lowest energy of optical phonon branches. These facts indicate that the LEMs are originated from one-phonon excitation. As seen in Fig. 6, the energy of the LEMs for 1*H*-CaAlSi and SrAlSi is close to that of low-lying phonon branch along H-L lines (bold lines in Fig. 6). The low-lying phonon branch is predominantly composed by out-of-plane displacement of Al atoms (see Fig. 7).

Even if we accept that the LEMs are the low-lying phonons, two problems still remain. One is a broken wave vector conservation. This means that another excitations must accompany to conserve wave vector as mentioned for the temperature dependence of intensity. The second problem is the relatively sharp peak structures of LEM. If the low-lying phonon modes with any wave vector are excited, the resulting spectra become a broad peak. The peak structures in the experiments indicate that the modes with some limited wave vectors are selectively excited. The wave vectors are selected by the accompanied excitations. Moreover, energy of the accompanied excitations must be very low, almost zero, because the observed energy, which is a sum of energies of the phonon modes and the accompanied excitations, is close to that of the phonon modes. Therefore, we conclude that the accompanied excitations are electronic excitations on the Fermi surface, which relate to the Friedel oscillation or charge fluctuation. The electronic fluctuation will strongly couple to the low-lying phonon modes using electron-phonon interactions and lower the energy of the phonon modes. In this picture, the resonance can be caused by the Drude term in the dielectric tensor. It agrees with the experimental result that the intensity increases with decreasing excitation energy.

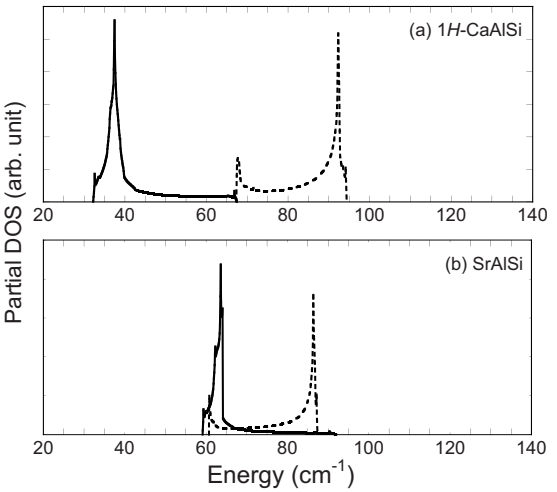

FIG. 8. Calculated partial phonon DOS, $D(\omega, q_z=0.5)$ (solid lines) and $D(\omega, q_z=0.25)$ (dashed lines), of 1*H*-CaAlSi (top) and SrAlSi (bottom).

According to the above-mentioned mechanism, we could approximately write a scattering intensity $I(\omega)$ of LEM at the energy ω as

$$I(\omega) = I_0 \int d^3q \int d^3q' g(q)^2 \delta[\omega - \omega_0(q)] \delta[\varepsilon(q') - \varepsilon(q+q')] \delta[\varepsilon(q') - \varepsilon_F], \quad (2)$$

where $\omega_0(q)$ and $\varepsilon(q)$ are energy of the low-lying phonon modes and energy of the conduction electrons with wave vector q, respectively, ε_F is the Fermi energy, and $g(q)$ is electron-phonon interaction coefficients. As seen in the phonon band structures, electron-phonon interactions strongly affect phonon energies on the plane $q_z=0.5$. Ignoring q dependence of $g(q)$ for simplicity, we get the following partial DOS for this contribution:

$$D(\omega, q_z = 0.5) = \int dq_x dq_y \delta[\omega - \omega_0(q)]. \quad (3)$$

Meanwhile, since the Fermi surface of both compounds has relatively flat planes near $q_z = \pm 0.125$, $D(\omega, q_z = \pm 0.25)$ should be also considered where wave vectors on the plane $q_z = \pm 0.25$ can connect two plane $q_z = \pm 0.125$. Thus, using $D(\omega, q_z=0.25) = D(\omega, q_z=-0.25)$, the Raman spectra are represented by $D(\omega, q_z=0.5) + 2D(\omega, q_z=0.25)$.

We show $D(\omega, q_z=0.5)$ and $D(\omega, q_z=0.25)$ for 1*H*-CaAlSi and SrAlSi in Fig. 8. For both compounds, two peaks are found and energy difference between them in SrAlSi is smaller than that in 1*H*-CaAlSi. Raman spectra of the LEMs were calculated by the convolution with the Lorenz function from for the obtained DOS. The resulting spectra are shown in Fig. 9, where a width of the Lorenz function is 10 cm^{-1}.

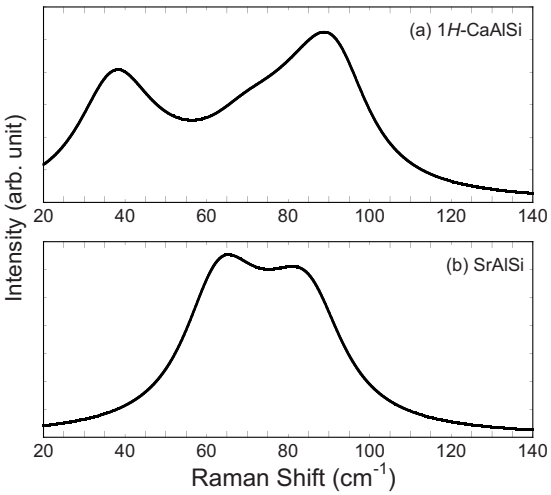

FIG. 9. Simulated Raman spectra for the LEM below 160 cm^{-1} for 1*H*-CaAlSi (top) and SrAlSi (bottom).

Agreement between the calculated spectra and the experimental results are well good in this rough estimation. Although the energy is lower than that of experiment by 20 cm^{-1} for SrAlSi, this discrepancy will be originated by the simplification of the Fermi surface.

Here, we also point out the large anharmonic contribution of LEMs as shown in Fig. 5. The anomalous energy decrease with decreasing temperature is probably explained by the quartic anharmonic potential model as in the caged compounds.[39–41] If the first-order contribution of the quartic anharmonic interactions dominates the energy, the phonon energy can be described by the form $\omega^2=\omega_0^2+k_4\langle u^2\rangle$, where ω_0 is the harmonic phonon energy depending on the volume, k_4 is a coefficient proportional to quartic anharmonic potential, and $\langle u^2\rangle$ is the square of thermal displacement. Since the LEMs are vibrations of Al atoms along the c axis, $\langle u^2\rangle$ is the atomic displacement parameter of Al atoms along the c axis. Synchrotron x-ray and neutron-diffraction structure analyses[15,16] have shown that the Al displacement parameter along the c axis in 1*H*-CaAlSi is estimated to be two times larger than that in SrAlSi at room temperature and that the Al displacement parameters along the c axis take very large values in comparison with the other displacement parameters. Therefore, the large $\langle u^2\rangle$'s produce the anomalous temperature dependence of energy through the anharmonic contribution of second term in above equation. This is consistent with our assignment of the LEMs. From above discussion, we conclude that the LEM arises from the resonance-scattering excitation of the low-lying phonon modes corresponding to the out-of-plane Al vibration with the large anharmonic contribution.

B. Energy difference at zone center

We next discuss the different phonon energy between $c(b^*,b^*)\bar{c}$ and $a(b^*,b^*)\bar{a}$ geometries in 1*H*-CaAlSi and SrAlSi as shown in Fig. 3. As discussed in Sec. III A, there are two possibilities to explain this anomalous result. One is the different surface structures between (001) and (100) surfaces. The other is the existence of the different energy modes depending on the propagation directions. Normally, it is impossible to explain the present experimental results using both possibilities.

In the former case, to reproduce the experimental difference, structural distortions near the surfaces must be very large, at least for one surface, while such evidence has neither been reported nor been observed at all. Notwithstanding this crucial difficulty for this scenario, it can straightforwardly show the doublet peaks due to the surface structure and the bulk part. Here, the E'_{high} modes are examined in this picture. For 1*H*-CaAlSi, two energies are observed: 442 and 457 cm^{-1}. The higher peak is found on the $c(b^*,b^*)\bar{c}$ spectra, while the lower peak is found on the $a(b^*,b^*)\bar{a}$ spectra and on the $c(b^*,b^*)\bar{c}$ spectra as low-energy shoulder. Recently, x-ray inelastic-scattering experiment[42] has been performed for 1*H*-CaAlSi and has revealed that the E'_{high} mode has only one energy about 440 cm^{-1} near the Brillouin-zone center. Penetration depth of x-ray is very long, about 0.7 mm for the experimental setting, compared to that of Raman-scattering experiments, about 1 μm typically. Thus the bulk energy of the E'_{high} mode is 440 cm^{-1}. Therefore, we can imagine that the (001) surface undergoes a large deformation and that the energy of the E'_{high} mode in the deformed surface is 457 cm^{-1}. The variation in spectral shape of the E'_{high} mode of the $c(a,a)\bar{c}$ spectra in Fig. 2(a) should be interpreted by a change in penetration depth, which varies with respect to the wavelength of the incident light. We note again that any structural distortion near surfaces over a large depth (1 μm order) has not been observed. Therefore, we cannot take this picture.

The latter case is also unacceptable at a glance because the scattering vectors are too small to reproduce the experimental difference. It is very unlikely that phonon energies with a wave vector about 10^{-3} $Å^{-1}$ in Raman scattering can be distinguished from their energies at the Brillouin-zone center. However, recently published papers[43–45] for MgB_2 have revealed that phonon self-energies can be drastically modified by including dynamical effect of electronic excitations if we consider a very small phonon wave vector as in Raman scattering. The effect of electronic dynamics depends on both length and direction of a phonon wave vector. The effect may be possible to explain the anomalous features in the present results: the different spectra between $a(b^*,b^*)\bar{a}$ and $c(b^*,b^*)\bar{c}$ geometries and the line shapes depending on the incident wavelength. Therefore, including an examination of this theory for this system, further theoretical works will give us the origin of the anomalous results presented here.

V. SUMMARY

We have shown the polarization, temperature, and excitation energy dependences of Raman-scattering measurements and *ab initio* calculations on 1*H*-CaAlSi and SrAlSi with $P\bar{6}m2$ symmetry to obtain the first information of the phonon properties. The E'_{low} and E'_{high} phonon modes required by Raman selection rule are clearly observed in both compounds. In particular, asymmetric line shape for E'_{high} modes

can be well described by the Fano model with the linewidth of ~ 10 cm^{-1}, which is drastically narrower than that of MgB_2. Thus, a quite different EPC to the in-plane bonding motion between MgB_2 and 1*H*-CaAlSi/SrAlSi has been found as expected by the theoretical calculations.

The LEMs are clearly observed below 160 cm^{-1} in addition to the Raman-active phonons. Comparing present Raman-scattering experiments with *ab initio* calculations allows us to assign the LEMs as the out-of-plane phonon modes of Al atom with the large anharmonicity through the resonance-scattering process. Furthermore, although the optical phonon at the Brillouin-zone center does not depend on the propagation directions, the anomalous phonon energy difference between propagation direction to the *c* axis and in plane is clearly observed. However, the origin of such an energy difference is still unclear and detailed theoretical investigations are necessary.

ACKNOWLEDGMENTS

This work was partly supported by the 21st COE program "High-Tech Research Center" Project for Private Universities matching fund subsidy from the Ministry of Education, Culture, Sports, Science and Technology of Japan (MEXT) (2002–2004), and a Grant-in-Aid for Scientific Research Priority Area "Skutterudite" (Grant No. 15072205).

[1] J. Nagamatsu, N. Nakagawa, T. Muranaka, Y. Zenitani, and J. Akimitsu, Nature (London) **410**, 63 (2001).
[2] A. Q. R. Baron, H. Uchiyama, Y. Tanaka, S. Tsutsui, D. Ishikawa, S. Lee, R. Heid, K.-P. Bohnen, S. Tajima, and T. Ishikawa, Phys. Rev. Lett. **92**, 197004 (2004).
[3] A. Shukla, M. Calandra, M. d'Astuto, M. Lazzeri, F. Mauri, C. Bellin, M. Krisch, J. Karpinski, S. M. Kazakov, J. Jun, D. Daghero, and K. Parlinski, Phys. Rev. Lett. **90**, 095506 (2003).
[4] H. J. Choi, D. Roundy, H. Sun, M. L. Cohen, and S. G. Louie, Phys. Rev. B **66**, 020513(R) (2002).
[5] Y. Kong, O. V. Dolgov, O. Jepsen, and O. K. Andersen, Phys. Rev. B **64**, 020501(R) (2001).
[6] J. Hlinka, I. Gregora, J. Pokorny, A. Plecenik, P. Kus, L. Satrapinsky, and S. Benacka, Phys. Rev. B **64**, 140503(R) (2001).
[7] D. A. Tenne, X. X. Xi, A. V. Pogrebnyakov, and J. M. Redwing, Phys. Rev. B **71**, 132512 (2005).
[8] H. Martinho, C. Rettori, P. G. Pagliuso, A. A. Martin, N. O. Moreno, and J. L. Sarrao, Solid State Commun. **125**, 499 (2003).
[9] K.-P. Bohnen, R. Heid, and B. Renker, Phys. Rev. Lett. **86**, 5771 (2001).
[10] J. W. Quilty, S. Lee, A. Yamamoto, and S. Tajima, Phys. Rev. Lett. **88**, 087001 (2002).
[11] T. E. Weller, M. Ellerby, S. S. Saxena, R. P. Smith, and N. T. Skipper, Nat. Phys. **1**, 39 (2005).
[12] M. Imai, E. Abe, J. Ye, K. Nishida, T. Kimura, K. Honma, H. Abe, and H. Kitazawa, Phys. Rev. Lett. **87**, 077003 (2001).
[13] M. Imai, El-Hadi S. Sadki, H. Abe, K. Nishida, T. Kimura, T. Sato, K. Hirata, and H. Kitazawa, Phys. Rev. B **68**, 064512 (2003).
[14] H. Sagayama, Y. Wakabayashi, H. Sawa, T. Kamiyama, A. Hoshikawa, S. Harjo, K. Uozato, A. K. Ghosh, M. Tokunaga, and T. Tamegai, J. Phys. Soc. Jpn. **75**, 043713 (2006).
[15] S. Kuroiwa, H. Sagayama, T. Kakiuchi, H. Sawa, Y. Noda, and J. Akimitsu, Phys. Rev. B **74**, 014517 (2006).
[16] S. Kuroiwa, T. Kakiuchi, H. Sagayama, H. Sawa, and J. Akimitsu, Physica C **460-462**, 154 (2007).
[17] I. I. Mazin and D. A. Papaconstantopoulos, Phys. Rev. B **69**, 180512(R) (2004).
[18] M. Giantomassi, Lilia Boeri, and G. B. Bachelet, Phys. Rev. B **72**, 224512 (2005).
[19] G. Q. Huang, L. F. Chen, M. Liu, and D. Y. Xing, Phys. Rev. B **69**, 064509 (2004).
[20] R. Heid, K.-P. Bohnen, B. Renker, P. Adelmann, T. Wolf, D. Ernst, and H. Schober, J. Low Temp. Phys. **147**, 375 (2007).
[21] C. S. Lue, B. X. Xie, and C. P. Fang, Phys. Rev. B **74**, 014505 (2006).
[22] R. Prozorov, T. A. Olheiser, R. W. Giannetta, K. Uozato, and T. Tamegai, Phys. Rev. B **73**, 184523 (2006).
[23] S. Tsuda, T. Yokoya, S. Shin, M. Imai, and I. Hase, Phys. Rev. B **69**, 100506(R) (2004).
[24] A. K. Ghosh, Y. Hiraoka, M. Tokunaga, and T. Tamegai, Phys. Rev. B **68**, 134503 (2003).
[25] S. Kuroiwa, H. Takagiwa, M. Yamazawa, J. Akimitsu, K. Ohishi, A. Koda, W. Higemoto, and R. Kadono, J. Phys. Soc. Jpn. **73**, 2631 (2004).
[26] X. Gonze, J.-M. Beuken, R. Caracas, F. Detraux, M. Fuchs, G.-M. Rignanese, L. Sindic, M. Verstraete, G. Zerah, F. Jollet, M. Torrent, A. Roy, M. Mikami, Ph. Ghosez, J.-Y. Raty, and D. C. Allan, Comput. Mater. Sci. **25**, 478 (2002).
[27] The ABINIT code is a common project of the Universite Catholique de Louvain, Corning Incorporated and other contributions, www.abinit.org
[28] J. P. Perdew and Y. Wang, Phys. Rev. B **45**, 13244 (1992).
[29] N. Troullier and José Luriaas Martins, Phys. Rev. B **43**, 1993 (1991).
[30] M. Fuchs and M. Scheffler, Comput. Phys. Commun. **119**, 67 (1999).
[31] A. Baldereschi, Phys. Rev. B **7**, 5212 (1973).
[32] D. J. Chadi and M. L. Cohen, Phys. Rev. B **8**, 5747 (1973).
[33] X. Gonze, Phys. Rev. B **55**, 10337 (1997).
[34] X. Gonze and C. Lee, Phys. Rev. B **55**, 10355 (1997).
[35] O. Jepson and O. K. Andersen, Solid State Commun. **9**, 1763 (1971).
[36] G. Lehmann and M. Taut, Phys. Status Solidi B **54**, 469 (1972).
[37] U. Fano, Phys. Rev. **124**, 1866 (1961).
[38] K. V. Klein, in *Light Scattering in Solids I*, edited by M. Cardona (Springer-verlag, Hedelberg, 1983).
[39] Y. Takasu, T. Hasegawa, N. Ogita, M. Udagawa, M. A. Avila, K. Suekuni, I. Ishii, T. Suzuki, and T. Takabatake, Phys. Rev. B **74**, 174303 (2006).
[40] T. Hasegawa, Y. Takasu, N. Ogita, M. Udagawa, J. I. Yamaura, Y. Nagao, and Z. Hiroi, Phys. Rev. B **77**, 064303 (2008).
[41] M. Udagawa, T. Hasegawa, Y. Takasu, N. Ogita, K. Suekuni,

M. A. Avila, T. Takabatake, Y. Ishikawa, N. Takeda, Y. Nemoto, and T. Goto, J. Phys. Soc. Jpn. **77**, 142 (2008).
[42] S. Kuroiwa, A. Q. R. Baron, T. Muranaka, R. Heid, K.-P. Bohnen, and J. Akimitsu, Phys. Rev. B **77**, 140503(R) (2008).
[43] M. Calandra and F. Mauri, Phys. Rev. B **71**, 064501 (2005).
[44] E. Cappelluti, Phys. Rev. B **73**, 140505(R) (2006).
[45] M. Calandra, M. Lazzeri, and F. Mauri, Physica C **456**, 38 (2007).